INFLUENCE OF CARBON NANOTUBES ON STIFFNESS PROPERTIES OF MULTISCALE COMPOSITE BLADES HAVING AIRFOIL-SHAPE CROSS-SECTION

Rafiee, M[1]*, Nitzsche, F[2], Labrosse, MR[1]
[1] Department of Mechanical Engineering, University of Ottawa, 161 Louis Pasteur, Ottawa, ON K1N 6N5, Canada
[2] Department of Mechanical and Aerospace Engineering, Carleton University, 1125 Colonel By Drive, Ottawa, ON K1S 5B6, Canada
* Corresponding author (mrafiee@uottawa.ca, mrafiee20@gmail.com)

Keywords*: CNTs-reinforced multiscale composites, beam cross-section, stiffness*

ABSTRACT

Microfiber-reinforced polymer composites reinforced with carbon nanotubes (CNTs), known as ‘‘multiscale” composites are a new generation of advanced composite materials and have received significant attention in the field of advanced, high-performance materials. In the present study, we numerically investigated the effects of CNTs on the stiffness properties of fiber-reinforced multiscale composite beams of general cross-sectional shapes and arbitrary anisotropic material properties. The three dimensional strain field was formulated in terms of one-dimensional strains and a three-dimensional warping displacement. The bulk material properties of the multiscale composite were predicted using the Halpin–Tsai equations and fiber micromechanics. The carbon nanotubes were assumed to be uniformly distributed and randomly oriented throughout the polymer matrix. The Variational Asymptotic Beam Section (VABS) method was used to numerically evaluate the stiffness and mass matrices of four test cases: strip, circular pipe, box beam and airfoil. Through a detailed parametric study, it was determined that inclusion of a small weight percentage of carbon nanotubes in the polymer matrix may be sufficient to significantly enhance the stiffness properties of fiber-reinforced composites.

1 INTRODUCTION

During the past decade, there has been a phenomenal growth in research activities to develop a methodology to analyze composite tailored beams and blades. Composite blades are, in general, built-up structures made of different materials. They are three dimensional (3D) bodies in which one dimension is large compared to the other two. This enables the separation of the 3D problem into two parts: a 2D local deformation field within the cross-section that is used to calculate the section properties, and a 1D global deformation field that is used to calculate the response of the beam [1]. The cross-sectional properties can be obtained using either ad hoc assumptions (e.g. [2]–[4]) or asymptotic methods (e.g. [1], [5]–[7]). In general, a fully populated matrix of cross-sectional stiffness properties is expected [8]. Analytical analyses are available for simple geometries; however, arbitrary cross-sections require numerical solutions such as finite element analysis (FEA). One of the most common FEA-based tools is the Variational Asymptotic Beam Section (VABS) [9]–[11]. The mathematical basis of VABS is the variational asymptotic method (VAM). VAM allows one to replace a three-dimensional structural model with a reduced-order model in terms of an asymptotic series of certain small parameters inherent to the structure [5]. Based on this method, Hodges and his coworkers developed theoretical foundations for the analysis of anisotropic composite beams [7]–[9], [12]–[14]. Many researchers extended the research done by Hodges [7], [15] to study the statics and dynamics of composite beams. For instance, Traugott et *al*. [16] developed a set of nonlinear, intrinsic equations describing the dynamics of beam structures undergoing large deformations of active helicopters blade. Their active structural model could be coupled with a suitable aerodynamic model for aeroelastic simulation

and aeroelastic control design. Ghorashi and Nitzsche [17] studied the nonlinear dynamic response of an accelerating composite rotor blade using perturbations. In another study, Ghorashi [18] also investigated the elasto-dynamic response of a rotating articulated blade. He used the linear VAM cross-sectional analysis, together with an improved damped nonlinear model for the rigid-body motion analysis of helicopter blades in coupled flap and lead-lag motions. Recently, Rafiee et al. [1] presented a computational model to investigate the static and vibration response of rotating and non-rotating nanocomposite beams and blades based on VAM.

Multiscale composites containing reinforcing elements at different length scales (i.e. macro, micro and/or nano) are a class of innovative and high-performance materials with a wide range of applications in the high-end industrial sectors [1], [19]. To date, multiscale composites have been developed using different types of nanomaterials. The most common are the nanomaterials with high aspect ratios such as nanotubes. Based on the Halpin–Tsai equations and fiber micromechanics, Rafiee et al. [1] investigated the statics and dynamics of carbon nanotubes reinforced composite cantilever beams. The large amplitude vibration of rectangular cross-section beams made of multiscale composites was also studied by He et *al*. [20].

To the best of authors' knowledge, there are presently no theoretical developments for the comprehensive cross-sectional analysis of multiscale composite blades. The beam cross-sectional analysis presented here investigates the effectiveness of CNTs reinforcements on the stiffness properties of beams and blades made of multiscale composite materials. The Halpin–Tsai equations and fiber micromechanics were used in hierarchy to predict the bulk material properties of the multiscale composite. The CNTs were assumed to be uniformly distributed and randomly oriented through the epoxy resin matrix. We used the VABS approach for numerical calculation of mass and stiffness matrices for four different cross sections: strip, circular pipe, box beam and airfoil. The volume fraction of fibers, the weight percentage of single-walled and multi-walled carbon nanotubes (SWCNTs and MWCNTs) were investigated through a detailed parametric study for their effects on the stiffness properties of composite beams and blades.

2 MATHEMATICAL MODELING

2.1 Material model

2.1.1 Strain energy

Under the condition of small local rotation, the three-dimensional strain field Γ_{ij} can be expressed as a 6 x 1 column matrix as: [8]

$$\hat{\Gamma} = \Gamma_h \hat{w} + \Gamma_\varepsilon \varepsilon + \Gamma_R \hat{w} + \Gamma_\ell \hat{w}' \tag{1}$$

where $\hat{w}$ is the warping function, ε is the 1D strain and matrices $\Gamma_h, \Gamma_\varepsilon, \Gamma_R,$ and Γ_ℓ are

$$\Gamma_h = \begin{bmatrix} 0 & 0 & 0 \\ \frac{\partial}{\partial\zeta_2} & 0 & 0 \\ \frac{\partial}{\partial\zeta_3} & 0 & 0 \\ 0 & \frac{\partial}{\partial\zeta_2} & 0 \\ 0 & \frac{\partial}{\partial\zeta_3} & \frac{\partial}{\partial\zeta_2} \\ 0 & 0 & \frac{\partial}{\partial\zeta_3} \end{bmatrix}, \quad \Gamma_\varepsilon = \frac{1}{\sqrt{g}} \begin{bmatrix} 1 & 0 & -\zeta_3 & \zeta_2 \\ 0 & \zeta_3 & 0 & 0 \\ 0 & -\zeta_2 & 0 & 0 \\ 0 & 0 & 0 & 0 \\ 0 & 0 & 0 & 0 \\ 0 & 0 & 0 & 0 \end{bmatrix},$$

$$\Gamma_R = \frac{1}{\sqrt{g}} \begin{bmatrix} \tilde{k} + k_1 I \left(\zeta_3 \frac{\partial}{\partial\zeta_2} - \zeta_2 \frac{\partial}{\partial\zeta_3} \right) \\ 0 \end{bmatrix}, \quad \Gamma_\ell = \frac{1}{\sqrt{g}} \begin{bmatrix} I \\ 0 \end{bmatrix},$$

$$\varepsilon = \begin{bmatrix} \gamma_{11} & \kappa_1 & \kappa_2 & \kappa_3 \end{bmatrix}^T, \quad \hat{w} = \begin{bmatrix} w_1 & w_2 & w_3 \end{bmatrix}^T,$$

$$\hat{\Gamma} = \begin{bmatrix} \Gamma_{11} & 2\Gamma_{12} & 2\Gamma_{13} & \Gamma_{22} & 2\Gamma_{23} & \Gamma_{33} \end{bmatrix}. \tag{2}$$

In Eq. (2), $\sqrt{g} = 1 - x_2 k_3 + x_3 k_2$, where k_α are the initial curvatures and the notation $\left(\ \right)$ forms an antisymmetric matrix from a vector according to $\left(\ \right) = -e_{ijk} \left(\ \right)_k$ using the permutation symbol e_{ijk} with $\left(\ \right)' = \frac{\partial}{\partial x_1}$. The internal energy density is defined by the strain energy associated with this strain field

$$2U = \left\langle \Gamma^T D \Gamma \right\rangle \tag{3}$$

where D is the 6 x 6 symmetric material matrix and the notation

$$\left\langle \bullet \right\rangle = \int_S \bullet \sqrt{g} \, \mathrm{d}x_2 \mathrm{d}x_3 = h^2 \int_S \bullet \sqrt{g} \, \mathrm{d}\zeta_2 \mathrm{d}\zeta_3 \tag{4}$$

The characteristic size of the domain S is denoted by h and the dimensionless coordinates $\zeta \equiv \left\{ \zeta_2 \equiv x_2 / h, \zeta_3 \equiv x_3 / h \right\}$ are introduced.

2.1.2 Discretization

The dimensional reduction from the original 3D structure to a 1D beam model can only be done approximately. As demonstrated in various applications, VAM can be used to construct a 1D formulation with minimum accuracy loss in comparison with the original 3D formulation. In order to deal with the arbitrary cross-sectional geometry and anisotropic materials, we need to turn to a numerical approach, such as FEA to find the warping functions. Therefore, we discretized the warping field using the finite element method at the cross-sectional level. By doing this, the unknown warping field was reduced to the displacements at the nodes of the mesh,

$$\hat{w}(x_1, x_2, x_3) = S(x_2, x_3)V(x_1), \tag{5}$$

with $S(x_2,x_3)$ representing the element shape functions and V as a column matrix of the nodal values of the warping functions over the cross-section. Substituting Eq. (5) into Eq. (1) and then into Eq. (3), we obtained

$$\begin{aligned} 2U = &\left(\frac{1}{h}\right)^2 V^T \langle [\Gamma_h S] D [\Gamma_h S] \rangle V \\ &+ \left(\frac{1}{h}\right) 2V^T \left(\langle [\Gamma_h S] D \Gamma_\varepsilon \rangle \varepsilon + \langle [\Gamma_h S] D [\Gamma_R S] \rangle V + \langle [\Gamma_h S] D [\Gamma_\ell S] \rangle V' \right) \\ &+ \varepsilon^T \langle [\Gamma_\varepsilon]^T D \Gamma_\varepsilon \rangle \varepsilon + V^T \langle [\Gamma_R S] D [\Gamma_R S] \rangle V + V'^T \langle [\Gamma_\ell S] D [\Gamma_\ell S] \rangle V' \\ &+ 2V^T \langle [\Gamma_R S] D [\Gamma_\varepsilon] \rangle \varepsilon + 2V'^T \langle [\Gamma_\ell S] D [\Gamma_\varepsilon] \rangle \varepsilon + 2V^T \langle [\Gamma_R S] D [\Gamma_\ell S] \rangle V' \end{aligned} \tag{6}$$

2.1.3 Stiffness matrix

Depending on how the displacement field component V is considered, different forms of strain energy can be derived. Herein, a known component of warping was assumed, which corresponded to a set of non-classical degrees of freedom (d.o.f.) in the final beam model. If Ψ_q is the column matrix with these assumed deformation modes, the decomposition of the warping field can be written as

$$V = \Psi_q q(x) + W(x) \tag{7}$$

The vector of modal amplitudes, q, is a column matrix of one or more new unknown functions, and W is the new warping to be found. Through integration by parts, the potential of the generalized Timoshenko model was written as

$$2U = \begin{bmatrix} \gamma_{11} \\ 2\gamma_{12} \\ 2\gamma_{13} \\ \kappa_1 \\ \kappa_2 \\ \kappa_3 \end{bmatrix}^T \begin{bmatrix} S_{11} & S_{12} & S_{13} & S_{14} & S_{15} & S_{16} \\ S_{21} & S_{22} & S_{23} & S_{24} & S_{25} & S_{26} \\ S_{31} & S_{32} & S_{33} & S_{34} & S_{35} & S_{36} \\ S_{41} & S_{42} & S_{43} & S_{44} & S_{45} & S_{46} \\ S_{51} & S_{52} & S_{53} & S_{54} & S_{55} & S_{56} \\ S_{61} & S_{62} & S_{63} & S_{64} & S_{65} & S_{66} \end{bmatrix} \begin{bmatrix} \gamma_{11} \\ 2\gamma_{12} \\ 2\gamma_{13} \\ \kappa_1 \\ \kappa_2 \\ \kappa_3 \end{bmatrix} \tag{8}$$

2.2 Material model

2.2.1 CNTs/fiber/polymer multi-scale composite material model

The three-phase multiscale composites considered herein comprised of isotropic matrix, CNTs and fibers and were assumed to be fabricated by dispersing nanotubes within an isotropic polymeric matrix and by impregnating the conventional fibers with this nanodispersed resin system. The alignment of fibers could be different for each lamina through the thickness. The CNTs were assumed to be isotropic and uniformly distributed and randomly oriented through the matrix. Bonding between CNTs and matrix, and the CNTs dispersion in the matrix were assumed to be perfect; each CNT had the same mechanical properties depending on the aspect ratio; all CNTs were straight rods; there was no void in the matrix; fiber-matrix bonding was assumed to be perfect. The constituent materials were assumed to be linear elastic throughout the deformation. The effective material properties of the three-phase CNTs/fiber/polymer multiscale laminated composite can be predicted according to a hierarchical combination of Halpin-Tsai and micromechanics approaches via two steps as shown in Figure 1.

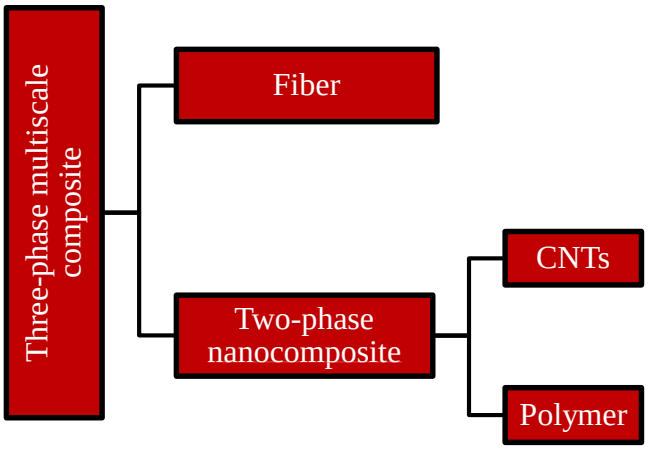

Figure 1. Hierarchy of the three-phase CNTs/fiber/polymer multiscale composites [21]

The effective material properties of the multiscale composite were assumed to be orthotropic and can be predicted by [21]

$$E_{11h} = V_F E_{11}^F + V_{MNC} E^{MNC}, \tag{9a}$$

$$\frac{1}{E_{22h}} = \frac{V_F}{E_{22}^F} + \frac{V_{MNC}}{E^{MNC}} - V_F V_{MNC} \frac{\nu_F^2 E^{MNC} / E_{22}^F + \nu_{MNC}^2 E_{22}^F / E^{MNC} - 2\nu^F \nu^{MNC}}{V_F E_{22}^F + V_{MNC} E^{MNC}} \tag{9b}$$

$$\frac{1}{G_{12h}} = \frac{V_F}{G_{12}^F} + \frac{V_{MNC}}{G^{MNC}}, \quad \nu_{12h} = V_F \nu^F + V_{MNC} \nu^{MNC}, \quad \rho_h = V_F \rho^F + V_{MNC} \rho^{MNC} \tag{9c}$$

where E_{11}^F, E_{22}^F, G_{12}^F, ν^F and ρ^F are Young's moduli, shear modulus, Poisson's ratio and mass density of the fibers, respectively, and E^{MNC}, G^{MNC}, ν^{MNC} and ρ^{MNC} represent the corresponding properties of the isotropic matrix of nanocomposite. V_F and V_{MNC} refer to the volume fractions of the fibers and the nanocomposite matrix, respectively.

According to the Halpin–Tsai equation, the tensile modulus of nanocomposites can be expressed as

$$E^{MNC} = \frac{E^{MER}}{8}\left[5\left(\frac{1+2\beta_{dd}V_{CN}}{1-\beta_{dd}V_{CN}}\right)+3\left(\frac{1+2\left(\frac{\ell^{CN}}{d^{CN}}\right)\beta_{dl}V_{CN}}{1-\beta_{dl}V_{CN}}\right)\right] \tag{10a}$$

$$\beta_{dl} = \frac{\left(\frac{E_{11}^{CN}}{E^{MER}}\right)-\left(\frac{d^{CN}}{4t^{CN}}\right)}{\left(\frac{E_{11}^{CN}}{E^{MER}}\right)+\left(\frac{\ell^{CN}}{2t^{CN}}\right)}, \quad \beta_{dd} = \frac{\left(\frac{E_{11}^{CN}}{E^{MER}}\right)-\left(\frac{d^{CN}}{4t^{CN}}\right)}{\left(\frac{E_{11}^{CN}}{E^{MER}}\right)+\left(\frac{d^{CN}}{2t^{CN}}\right)} \tag{10b}$$

where E_{11}^{CN}, V_{CN}, ℓ^{CN}, d^{CN} and t^{CN} are the Young's modulus, volume fraction, length, outer diameter and the thickness of carbon nanotubes, respectively, and V_{MER} and E^{MER} indicate the volume fraction and Young's modulus of the isotropic epoxy resin matrix, respectively.
The volume fraction of carbon nanotubes can be expressed as [21]

$$V_{CN} = \frac{w^{CN}}{w^{CN} + (\rho^{CN} / \rho^{MER}) - (\rho^{CN} / \rho^{MER}) w^{CN}}, \tag{11}$$

where w^{CN} is the mass fraction of the carbon nanotubes, ρ^{CN} and ρ^{MER} are the mass densities of the carbon nanotube and epoxy resin matrix, respectively.
Poisson's ratio and mass density ρ can be expressed as

$$\nu^{MNC} = \nu^{MER},\ \rho^{MNC} = V_{CN}\rho^{CN} + V_{MER}\rho^{MER} \tag{12}$$

where ρ^{CN}, ρ^{MER} are mass densities of the carbon nanotubes and matrix and ν^{MER} is Poisson's ratio for the epoxy resin matrix, respectively. As the amount of CNTs was small, Poisson's ratio for the CNT composite was assumed to be the same as that of epoxy, 0.33 [21].

3 NUMERICAL STUDY

The theoretical development presented in the previous section was numerically implemented in VABS. Not all stiffness components are shown since the stiffness matrix is symmetric. All results are given at the area centroid and the 6×6 stiffness matrix is arranged as 1: extension; 2: chordwise transverse shear; 3: flatwise transverse shear; 4: torsion; 5: flatwise bending; and 6: chordwise bending. It should be noted that stiffness components with relatively small values compared to the others are neglected in the tabular data and figures. In this study, Bell540 airfoil cross-section was considered. The geometric parameters, material properties and stacking sequences of Bell540 are given in Figure. 2 and Ref. [1] unless otherwise specified. The complete blade had a span of 0.8124 m (beyond the clamping area at the root). A finite element mesh with 9,885 6-noded triangular elements (40,850 d.o.f.) was used. The predicted stiffness coefficients are given in Figure. 3. The beam exhibited extension-chordwise bending (S_{16}) and flatwise transverse shear-twist (S_{34}) couplings.

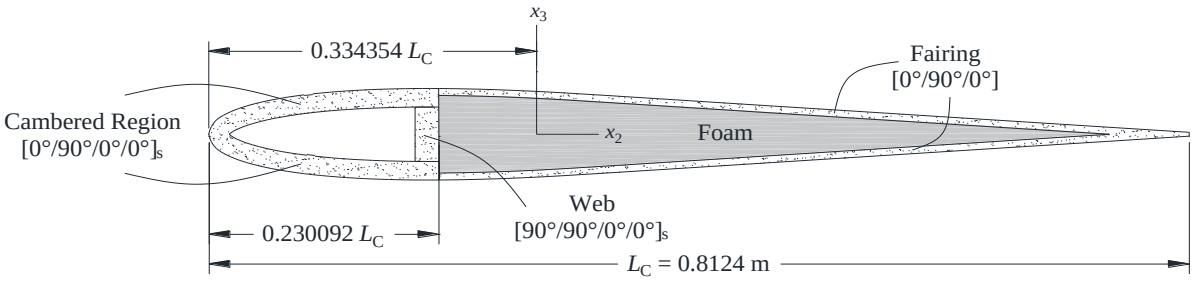

Figure. 2. Profile of the Bell540 airfoil blade and ply-up.

The results from Figure. 3 reveal that the most significant coupling terms were extension (S_{11}), chordwise transverse shear (S_{22}) and extension- chordwise bending (S_{16}). The reinforcement achieved by MWCNTs is much lower than that by SWCNTs. Nevertheless, MWCNTs can still be an interesting choice due to the higher cost of large scale use of using SWCNTs in mass production applications.

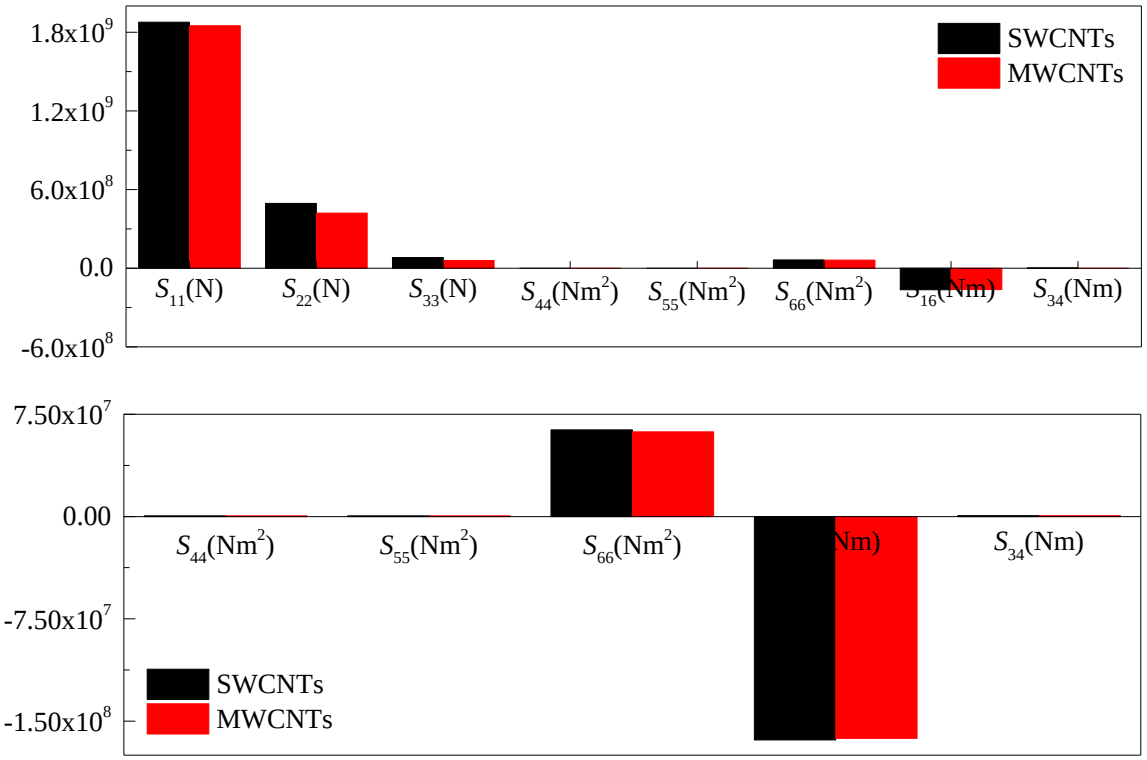

Figure. 3. Effect of CNTs structure on the stiffness properties per unit length of Bell540 airfoil configuration (w^{CN} =1%, $\mu \approx$ 2.9376 kg/m, $\bar{x}_2 = \bar{x}_3$ =0., i_2=1.354×10^{-3} kgm, i_3=3.315 ×10^{-3} kgm, i_{23}=0 kgm)

4 CONCLUSIONS

A finite-element-based, cross-sectional analysis for CNTs-reinforced multiscale composite beams was formulated from geometrically nonlinear, 3D elasticity. The 3D strain field was formulated in terms of 1D generalized strains and a 3D warping displacement. The developed formulation was numerically implemented in the VABS to compute the cross-section stiffness matrices and mass properties. The results indicated that the inclusion of a small weight percentage of carbon nanotubes in the polymer matrix was sufficient to induce a significant improvement in stiffness properties. In some cases, however, CNTs may be used to weaken some specific structural couplings. SWCNTs were shown to have more significant effects than MWCNTs on the stiffness properties. This may be due to lower specific surface area and defect structure of MWCNTs. Overall, CNTs can be used to tailor the design of beams and blades for specific stiffness properties.

5 REFERENCES

[1] M. Rafiee, F. Nitzsche, and M. Labrosse, “Rotating nanocomposite thin-walled beams undergoing large deformation,” *Compos. Struct.*, vol. 150, pp. 191–199, 2016.

[2] S. N. Jung, V. T. Nagaraj, and I. Chopra, “Refined Structural Model for Thin- and Thick-Walled Composite Rotor Blades,” *AIAA J.*, vol. 40, no. 1, pp. 105–116, 2002.

[3] O. Song and L. Librescu, “Structural Modeling and Free Vibration Analysis of Rotating Composite Thin-Walled Beams,” *J. Am. Helicopter Soc.*, vol. 42, no. 4, p. 358, 1997.

[4] P. F. Pai and A. H. Nayfeh, “Three-Dimensional Nonlinear Vibrations of Composite Beams - I. Equations of Motion,” *Nonlinear Dyn.*, vol. 1, pp. 477–502, 1990.

[5] V. Berdichevsky, E. Armanios, and A. Badir, “Theory of anisotropic thin-walled closed-cross-section beams,” *Compos. Eng.*, vol. 2, no. 5–7, pp. 411–432, 1992.

[6] C. E. S. Cesnik and S. Shin, “On the modeling of integrally actuated helicopter blades,” *Int. J. Solids Struct.*, vol. 38, no. 10–13, pp. 1765–1789, Mar. 2001.

[7] D. H. Hodges, “Geometrically Exact , Intrinsic Theory for Dynamics of Curved and Twisted Anisotropic Beams,” *AIAA J.*, vol. 41, no. 6, pp. 1131–1137, 2003.

[8] D. H. Hodges, *Nonlinear Composite Beam Thery*. AIAA, 2006.

[9] C. E. S. Cesnik and D. H. Hodges, “VABS: A New Concept for Composite Rotor Blade Cross-Sectional Modeling,” *J. Am. Helicopter Soc.*, vol. 42, p. 27, 1997.

[10] W. Yu, D. H. Hodges, and J. C. Ho, “Variational asymptotic beam sectional analysis - An updated version,” *Int. J. Eng. Sci.*, vol. 59, pp. 40–64, 2012.

[11] W. Yu, “VABS Manual for Users,” *Dep. Mech. Aerosp. Eng. Utah State Univ. Logan, Utah*, pp. 1–22, 2011.

[12] A. R. Atilgan and D. H. Hodges, “Unified nonlinear analysis for nonhomogeneous anisotropic beams with closed cross sections,” *AIAA J.*, vol. 29, no. 11, pp. 1990–1999, Nov. 1991.

[13] F. Jiang, W. Yu, and D. H. Hodges, “Analytical Modeling of Trapeze and Poynting Effects of Initially Twisted Beams,” *J. Appl. Mech.*, vol. 82, no. 6, p. 61003, Jun. 2015.

[14] D. H. Hodges, “Modeling of Composite Beams and Plates for Static and Dynamic Analysis,” 1990.

[15] D. H. Hodges, “A mixed variational formulation based on exact intrinsic equations for dynamics of moving beams,” *Int. J. Solids Struct.*, vol. 26, no. 11, pp. 1253–1273, 1990.

[16] J. P. Traugott, M. J. Patil, and F. Holzapfel, “Nonlinear modeling of integrally actuated beams,” *Aerosp. Sci. Technol.*, vol. 10, no. 6, pp. 509–518, 2006.

[17] M. Ghorashi and F. Nitzsche, “Nonlinear dynamic response of an accelerating composite rotor blade using perturbations,” *J. Mech. Mater. Struct.*, vol. 4, no. 4, pp. 693–718, 2009.

[18] M. Ghorashi, “Nonlinear analysis of the dynamics of articulated composite rotor blades,” *Nonlinear Dyn.*, vol. 67, pp. 227–249, 2012.

[19] M. Kim, Y. Bin Park, O. I. Okoli, and C. Zhang, “Processing, characterization, and modeling of carbon nanotube-reinforced multiscale composites,” *Compos. Sci. Technol.*, vol. 69, no. 3–4, pp. 335–342, 2009.

[20] X. Q. He, M. Rafiee, S. Mareishi, and K. M. Liew, “Large amplitude vibration of fractionally damped viscoelastic CNTs/fiber/polymer multiscale composite beams,” *Compos. Struct.*, vol. 131, pp. 1111–1123, Nov. 2015.

[21] M. Rafiee, X. Q. He, S. Mareishi, and K. M. Liew, “Modeling and stress analysis of smart CNTs/fiber/polymer multiscale composite plates,” *Int. J. Appl. Mech.*, vol. 6, no. 3, p. 1450025, 2014.